SEMI-EMPIRICAL HEAT TRANSFER CORRELATIONS IN COMBUSTION CHAMBERS FOR TRANSIENT SYSTEM MODELLING

Francesco Di Matteo[†], Marco De Rosa[‡*], Marcello Onofri[†]
[†]Sapienza University of Rome
Dipartimento di Meccanica e Aeronautica, Via Eudossiana 18, I-00184 Rome, Italy
[‡]ESA-ESTEC, Propulsion Engineering
Keplerlaan 1, 2201AZ Noordwijk, Netherlands

Abstract

In order to contain the extreme temperature conditions in a combustion chamber of a liquid rocket engine, a plethora of different technologies have been developed over the years (film cooling, ablative cooling, thermal barrier coating, regenerative cooling, radiative cooling...). Each one of these requires specific modelling. The available system modelling tools for transient analysis use overly simplified heat transfer models, often disregarding the particular cooling technique to be simulated. It is therefore necessary to refine these models to obtain more capabilities, using specific models for each cooling system adopted.

EcosimPro is an object oriented tool capable of modelling various kinds of dynamic systems. The correlations described within this paper are implemented alongside ESPSS, a propulsion system library compatible with EcosimPro. This paper describes several implementations of heat transfer correlations to transient problems, applied to combustion chambers and their cooling systems. Development of a detailed injector layout, implementation of different heat transfer correlations, and a quasi-2D fluid flow model for regenerative cooling channels will be simulated and the results will be compared between them and data from literature.

Nomenclature

A	Area, m^2
t	Material thickness, m
C_p	Specific heat, J/kg·K
h_c	Convective heat transfer coefficient, W/m^2·K
M	Mass, kg
$\dot{m}$	Mass flow rate, kg/s
$\dot{q}$	Heat flux, W/m^2
T	Temperature, K
λ	Thermal conductivity, W/m·K
μ	Dynamic viscosity, Pa·s
ξ	Friction coefficient, -
ρ	Density, kg/m^3
σ	Radiative heat transfer coefficient, W/m^2·K^4
τ	Shear stress flux, Pa
St	Stanton number, -
Re	Reynolds number, -
Pr	Prandtl number, -

Subscript

aw	adiabatic wall
cap	capacity
cav	cavity
$cond$	conductive
$conv$	convective
inj	injector
hg	hot gas
rad	radiative
ref	reference condition
t	turbulent
th	throat condition
w	wall

*Corresponding author: marco.de.rosa@esa.int

1 Introduction

The European Space Propulsion System Simulation libraries (ESPSS) have been developed by Iberespacio in the frame of two ESA contracts in the last 3 years, and enable the modelling and analysis of propulsion systems for both spacecraft and launcher applications. The combustion chamber heat transfer models available in ESPSS are discussed and improved in the present paper.

Three new, more complex and accurate models will be presented in Section 2: the first one for the injector plate, a second one for the evaluation of the heat transfer coefficient on the hot gas side of the thrust chamber, and the third one for the evaluation of the thermal stratification inside high aspect ratio cooling channels (HARCC).

Each model will be tested or validated in Section 3, with relevant test cases.

2 Models

2.1 Injector plate

Original design

The original injector plate model present in the ESPSS library features a very simplified thermal model. Indeed the injector plate topology takes into account the effects of the radiative heat transfer, but the conductive and convective heat fluxes are evaluated using only a virtual conductance. As in Figure 1(a) the original injector plate is built by a radiative and a conductive component linked upstream in parallel directly to the combustor hot gases. These two components are linked to a capacitive component, used to simulate the thermal inertia of the injector cavity walls. This heat capacity is then connected to the two fluid cavities.

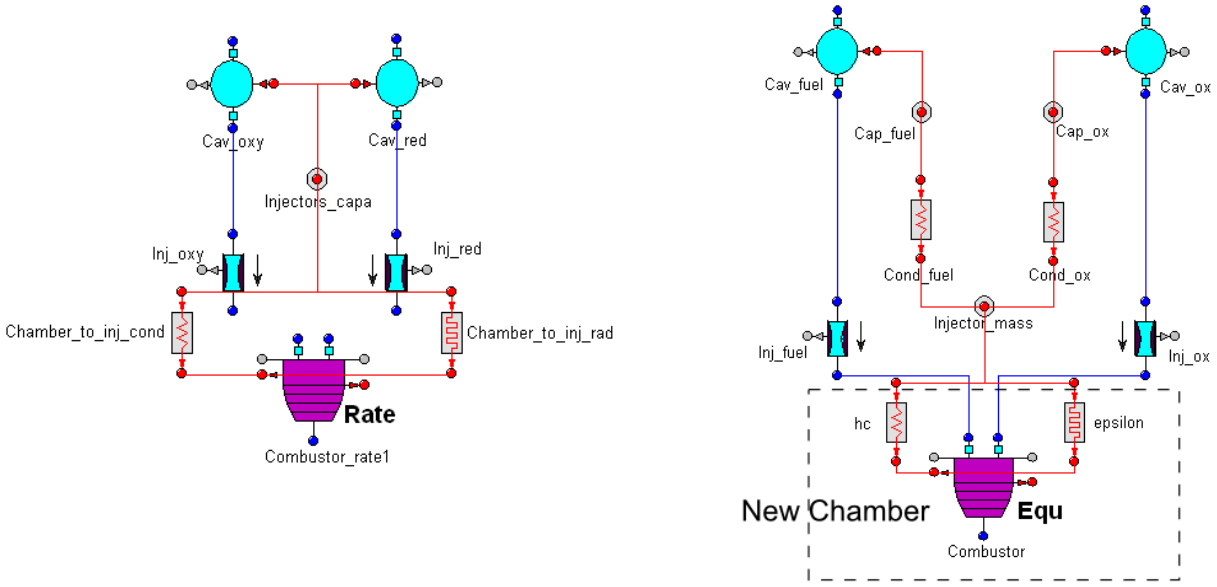

(a) topology schematic of the original injector plate

(b) topology schematic of the new injector plate

Figure 1: schematics of the injector plates

In this way it is not possible to evaluate the presence of convective heat transfer and to take into account the correct effect of the conductive and capacitive behaviour of the injector plate material. Moreover, the core temperature in the first volume of the chamber is considered as the wall temperature of the injector plate, and this is unrealistic.

New design

For this reason, the possibility to implement an upgraded version of the injector plate topology inside the ESPSS library has been investigated. The aim of this new model is to take into account the convective and radiative heat transfer between the fluid in the first volume of the chamber and the face plate, and evaluate the conductive and capacitive effect of the injector walls in more accurate way, representative of a generic injector head. The new structure of the injector plate (see Figure 1(b)) wants to maintain the level of simplicity of the original model in order to keep the computational cost low, and to be applicable to several different injector geometries (impinging, coaxial, etc…), but in the same time wants also to improve the heat transfer characteristics from the chamber to the injector cavities. In the first volume of the chamber the convective and radiative heat fluxes to the injector face are evaluated:

$$\dot{q}_{conv} = h_{c,hg}\left(T_{aw} - T_{w,hg}\right) \tag{1}$$

$$\dot{q}_{rad} = \sigma\left(T_{core}^4 - T_{w,hg}^4\right) \tag{2}$$

using the mass and the material properties of the injector plate (heat capacity, thermal conductivity) the model evaluates the conductive heat transfer and capacity effect of the walls:

$$\dot{q}_{cond}|_{ox,fu} = \left(\frac{\lambda}{t_{ox,fu}}\right)\left(T_{w,hg} - T_{w,cav}\right) \tag{3}$$

and for the capacitive components

$$\dot{q}_{cap,hg} = \dot{q}_{cond,ox} + \dot{q}_{cond,fu} + \dot{q}_{conv} + \dot{q}_{rad} \tag{4}$$

$$\dot{q}_{cap,ox} = \dot{q}_{cond,ox} + \dot{q}_{cav,ox} \tag{5}$$

$$\dot{q}_{cap,fu} = \dot{q}_{cond,fu} + \dot{q}_{cav,fu} \tag{6}$$

$$\dot{q}_{cap,k} = c_p M \frac{dT}{dt} \qquad \text{with} \quad k = hg, ox, fu; \tag{7}$$

The thermal conductivity and heat capacity values are function of the chosen material of the injector plate and of its temperature. For simplicity reasons the injector plate is assumed to be made of only one material. The thickness t used for the evaluation of the conductive heat flux has to be considered as a "characteristic" injector head thickness or width, and presents two different values, one for the ox side and the other for the fuel side. Please note that the capacitive components for each propellant side are divided in two parts in order to obtain three different temperatures: $T_{w,hg}$, $T_{ox,cav}$, $T_{fu,cav}$, respectively the temperature of the injector plate on the hot side, the oxidizer and the fuel cavity wall temperature on the cold fluid side.

2.2 Heat transfer coefficient correlations

In the ESPSS library the heat transfer coefficient inside the combustion chamber is evaluated using the well-known Bartz

correlation [2]. The original formulation of this equation does not take into account several aspects, such as the combustion zone due to atomization, vaporization and combustion delays in the proximity of the injector plate, the boundary layer growth through the cylindrical part of the chamber, the correct evaluation of the flow acceleration in the convergent-divergent part of the nozzle, etc...

The heat flux in ESPSS takes into account the convective and radiative phenomena:

$$\dot{q}_{wall} = h_c A_{wet}(T_{aw} - T_w) + \sigma A_{wet}(T_{core}^4 - T_w^4) \quad (8)$$

The heat transfer coefficient h_c can now be evaluated by different correlations; the equations have been implemented in a modular way in order to allow the implementation of further models in the future and to let the user choose the best one by the use of the graphical user interface as shown in Figure 2.

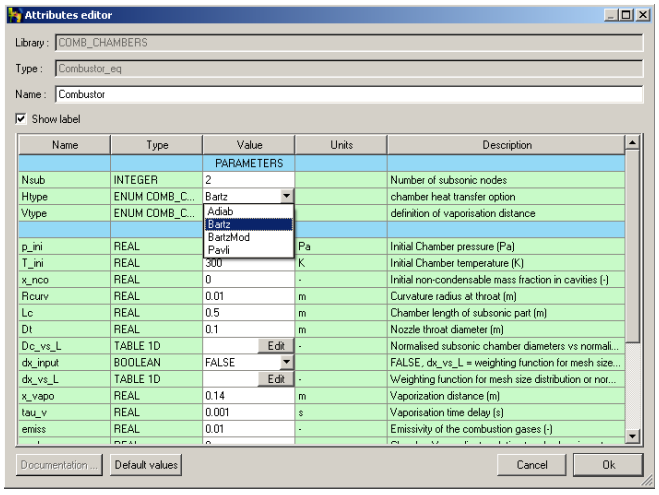

Figure 2: New graphical user interface

Since many correction factors used in literature are based on Stanton type correlations, it was decided to use this kind of dimensionless number to evaluate the heat transfer coefficient.

$$St = \frac{h_c}{\rho_\infty v_\infty c_{p,ref}} = \frac{\dot{q}}{\rho_\infty v_\infty c_{p,ref}(T_{aw} - T_w)} \quad (9)$$

the Stanton number represents the ratio between heat transferred to a fluid and the thermal capacity of this fluid. In the combustion chamber component three different correlations have been implemented:

- Original Bartz Equation
- Modified Bartz Equation
- Pavli Equation

In order to use the Bartz equation with Stanton type correction factors, the Bartz equation has been rewritten as a Stanton type equation:

$$St_{Bartz} = 0.026 \left(\frac{\mu_{ref}^{0.2}}{c_{p,ref}^{0.6}} \right) \left(\frac{\lambda_{ref}}{\mu_{ref}} \right)^{0.6} (\dot{m})^{-0.2} A^{0.1} \left(\frac{\pi/4}{R_{curv} D_{th}} \right)^{0.1} \quad (10)$$

To improve the behaviour of the original Bartz equation, a temperature correction factor K_T was added, taking into account that the new reference temperature is calculated halfway between the wall and the free stream static temperature. Moreover, since the geometric reference parameter in the original Bartz equation was the throat diameter, a further correction factor K_x was added for the consideration of the boundary layer growth in the cylindrical part and in the nozzle [1]:

$$K_T = \left(\frac{T_{aw}}{T_{ref}} \right)^a \qquad K_x = \left(\frac{x}{x_{th}} \right)^b \quad (11)$$

hence, the Stanton type modified Bartz equation becomes:

$$St_{Bartz,mod} = St_{Bartz} K_T K_x \quad (12)$$

Because of its simplicity, the Pavli equation has been implemented as well. The Pavli equation including the two correction factors discussed before is [4], [1]:

$$St_{Pavli} = 0.023 Re^{-0.2} Pr^{-0.6} \left(\frac{T_{aw}}{T_{ref}} \right)^e \left(\frac{x}{x_{th}} \right)^f \quad (13)$$

The Reynolds number Re is calculated with respect to the local chamber diameter and the property reference temperature is an averaged boundary layer temperature. In this equation the temperature correction factor and the streamwise correction factor are also included.

In order to improve the heat flux model in the combustion chamber another correction factor was added taking into account the vaporization phenomenon near the injector plate. In the so-called *combustion zone* the heat flux decreases when getting closer to the injector plate. This behaviour is due to the incomplete mixing and reaction of the flow for the given injector and combustion chamber. The mixing region has a finite length where the combustion is less effective, therefore the heat fluxes are lower. This correction factor is applied by using a Stanton type correlation derived from Bartz or Pavli equations. To generate a specific correction factor a new flag is added in the graphical interface (see Figure 2); the user can choose to use his own value of the combustion length or compute the combustion zone by a geometrical correlation. In the latter case, to generate a specific correction factor two steps are required: first, the length of this combustion zone x_{max} has to be calculated based on the injector plate geometry; then a functional dependency of the heat flux in the range $x_0 \leq x \leq x_{max}$ has to be found.

Once the combustion zone length is evaluated it is possible to calculate a correction factor by means of a tangential Stanton number dependency [1]:

$$\frac{St^*(x)}{St(x_{max})} = \frac{1}{4} \arctan \left[7 \left(\frac{x}{x_{max}} - 0.63 \right) \right] + 0.7 \quad (14)$$

The last correction factor added to achieve a better agreement between the numerical and the experimental results is a correction factor K_{acc} related to the *flow acceleration*. In fact, the measured heat fluxes are lower than the calculated ones upstream and downstream the nozzle throat.

The behaviour is caused probably by the nozzle contour and therewith due to the flow acceleration (bigger boundary layer thickness). Instead of using the local velocity gradient to develop the correction factor, a more practicable way is to use the absolute value of the first derivative of the chamber radius with respect to the streamwise coordinate, $|dr/dx|$.

The correction factor K_{acc} requires two boundary conditions. In the cylindrical part K_{acc} should be equal to 1. The other boundary condition is described by $K_{acc} = 0$ and represents the disappearance of convective heat transfer due to flow separation. The following correction is used to take into account both conditions [1]:

$$St^* = St \cdot K_{acc} = St \cdot \sqrt{1 - \left|\frac{dr}{dx}\right|} \tag{15}$$

2.3 Q-2D model for cooling channels

For new engines the use of HARCC (High Aspect Ratio Cooling Channels) is necessary. Indeed, the use of these kinds of channels permits a lower wall temperature and a longer life. Beside these advantages, the HARCC have as usual also drawbacks: the pressure drop is higher and thermal stratification occurs within them. In order to optimize the design of this kind of channels it is fundamental to evaluate the thermal stratification effect and so the heat absorption of the coolant. As compared to two different papers from the Department of Mechanics and Aeronautics (DMA) of "Sapienza" University of Rome [5] and the German Aerospace Center (DLR) [10] that found their own way to analyse the HARCC, a new approach is here proposed to evaluate thermal stratification in system tools such as EcosimPro. Starting from the one dimensional governing equations present in the ESPSS library:

$$\frac{\partial \boldsymbol{u}}{\partial t} + \frac{\partial f(\boldsymbol{u})}{\partial x} = S(\boldsymbol{u}) \tag{16}$$

where

$$\boldsymbol{u} = A \begin{bmatrix} \rho \\ \rho x^{nc} \\ \rho v \\ \rho E \end{bmatrix}; \quad f(\boldsymbol{u}) = A \begin{bmatrix} \rho v \\ \rho v x^{nc} \\ \rho v^2 + P \\ \rho v H \end{bmatrix}; \tag{17}$$

$$S(\boldsymbol{u}) = \begin{bmatrix} -\rho A k_{wall}(\partial P/\partial t) \\ -\rho x^{nc} A k_{wall}(\partial P/\partial t) \\ -0.5(d\xi/dx)\rho\, v|v|A + \rho g A + P(dA/dx) \\ \dot{q}_w(dA_{wet}/dx) + \rho g v A \end{bmatrix} \tag{18}$$

The new code presents an unsteady Q-2D model and can be considered as an evolution of the two inspiring works presented by DMA and DLR. The control volumes are divided in slices, one on top of the other linked together longitudinally by the momentum and energy viscous fluxes. The mass conservation equation is written in a one-dimensional form but it is calculated for each slice, while the momentum and energy conservation equation are written in a quasi-2D form taking into account friction, longitudinal viscous transport, wall heat flux and longitudinal fluid heat flux respectively.

Equations (16),(17) have been modified in the following way, to obtain inside each channel several longitudinal fluid veins one on top of the other and linked by the momentum and energy viscous fluxes:

$$\frac{\partial \boldsymbol{u}}{\partial t} + \frac{\partial f(\boldsymbol{u})}{\partial x} + \frac{\partial g(\boldsymbol{u})}{\partial y} = S(\boldsymbol{u}) \tag{19}$$

where

$$g(\boldsymbol{u}) = A_{wet} \begin{bmatrix} 0 \\ 0 \\ \tau_{xy} \\ q_c \end{bmatrix}; \qquad \tau_{xy} = \mu_t \frac{\partial v}{\partial y}; \qquad q_c = \lambda_t \frac{\partial T}{\partial y} \tag{20}$$

The turbulent conductivity coefficient k_t is evaluated using the empirical correlation of Kacynski [3]. By the use of a constant turbulent Prandtl number we obtain the turbulent viscosity.

$$\frac{\lambda_t}{\lambda} = 0.008\, Re^{0.9} \qquad Pr_t = 0.9 \qquad \mu_t = \frac{Pr_t\, \lambda_t}{c_p} \tag{21}$$

Hence each slice has his own velocity, and no empirical correlations are used to evaluate the velocity profile being automatically related to the viscous fluxes and the longitudinal heat flux. To accurately describe the wall heat flux also the wall temperature is assumed to to vary along the *y* direction. All thermodynamic properties such as temperature, density and enthalpy depend on *x*, *y* and time.

Please note that it is the first time to our knowledge that a quasi-2D approach is implemented for pipe flows in a system tool for transient analysis; with this model we are able to evaluate not only the stratification effect but also the time that the coolant needs to show this stratification during the transient phase of the engine ignition.

3 Results

3.1 Injector plate validation

In order to validate the behaviour of the new injector plate model, a numerical approach has been used because no experimental results were found in open literature. A pressure fed propulsion system has been modelled and tested with both injector plate models. The test case represents a typical spacecraft propulsion system supplied by nitrogen tetroxide (NTO) as oxidiser, and monomethylhydrazine (MMH) as fuel. The system is designed in order to reach a chamber pressure of

$\approx$ 10 bar with a mixture ratio of 1.65 at steady state conditions.

Figure 3 compares the two models by assessing the thermal behaviour inside the injector cavities and the injector plate walls.

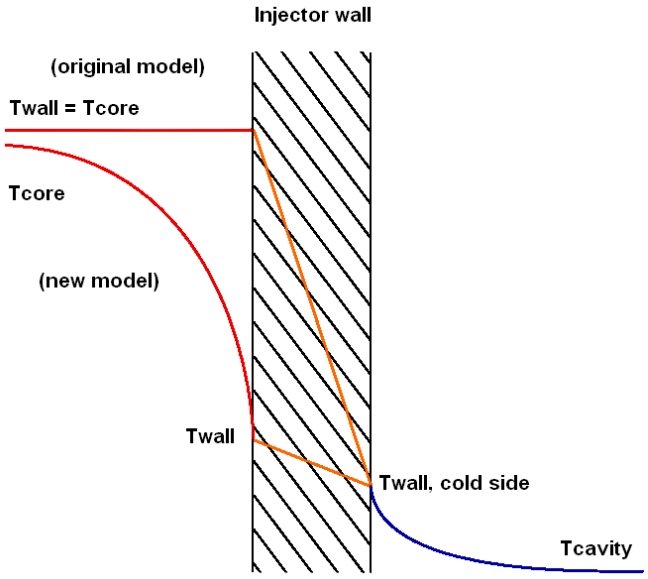

Figure 3: temperature profiles from original and new model

Table 1 summarizes the major features for each side of the injector plate evaluated by the new model at steady state conditions.

Table 1: injector plate variables comparison

Variable	Fuel	Oxidiser	Chamber
Input			
Propellant	MMH	N_2O_4	
Injector material	Titanium	Titanium	
Injector head mass [kg]			1.5
Injector head thickness [m]	0.001	0.003	
Injector head area [m^2]	0.023	0.023	0.023
Chamber pressure [bar]			9.85
Chamber temperature [K]			3002.8
Mixture ratio [$-$]			1.65
h_c coefficient [$W/m^2 \cdot K$]			450
Inlet temperature [K]	300	292.3	
Output			
Inj. heat flux [W]	17049	9835	26884
Cavities ΔT [K]	4.85	3.10	
$Wall_{c,hg}$ temperature [K]	440.8	402.3	493.7

It is evident that the temperature at injector plate wall in the original version of the model would have been unrealistic ($T_{hg} = T_c$). Only the presence of the virtual conductance allows the injector cavities not to increase the fluid temperature to unrealistic values.

Using the newly developed model, the software is able to deliver reasonable outputs with physically valid geometries. Moreover it is possible to obtain different cavities wall temperatures for each propellant side, while before it could not occur.

3.2 Heat transfer coefficient correlations

In the years 1999-2000, in the frame of an ESA GSTP-2 contract, Astrium performed a series of experiments with a water cooled calorimetric combustion chamber [1]. This section describes the results of using different correlations based on Bartz ([1],[2]) and Pavli ([1],[4]), and their comparison with the experimental results from this calorimetric chamber test campaign.

The calorimetric chamber is a subscale, water cooled thrust chamber with twenty segments [9]. Each segment features an independent water feed system with volume flow measurement.For each segment the heat flux is measured individually. Modelling of the described calorimetric system has been performed with EcosimPro, using the following components [9]:

- 1 combustion chamber with 21 nodes (component to validate)
- 20 regenerative circuits with 5 nodes each
- 20 mass flow regulated water feed lines (with the necessary junctions and boundary conditions)
- mass flow regulated propellant feed lines

The simulation was performed using the couple liquid oxygen/gaseous hydrogen as propellants, at an O/F ratio varying from 5 to 7 and at a total pressure from 35 to 70 bar in the combustor; for each test point the propellant mass flows are chosen in order to get the desired pressure and mixture ratio. In order to get the right pressure drop through the cooling circuit, the rugosities of the cooling channels had to be adapted. Values between 3.2 and 25 μm were chosen. This tuning was necessary because of the partially unknown layout of the cooling circuit and its feed lines (pipes, fittings, ...).

The heat fluxes calculated with every correlation described in modelling subsection are plotted in Figure 3(a) for the nominal case ($p = 60$ bar, $MR = 6$); in Figure 3(b) simulation results are compared to experimental data obtained varying the chamber pressure ($p = 35, 60, 70$ bar, $MR = 6$), Figure 3(c) shows the simulation and experimental comparison for tests with constant chamber pressure but different mixture ratio ($p = 60$ bar, $MR = 5, 7$), while in Figure 3(d) the hot gas wall temperature trend is shown at different chamber pressures. The correlations are all plotted with lines and experimental data with symbols.

The "Combustion zone" correction factor is able to represent the lower heat fluxes in the first part of the chamber. Unfortunately, the introduced correction cannot be considered predictive (that is, a correction that would give good results in a different combustion chamber and injector face): it would

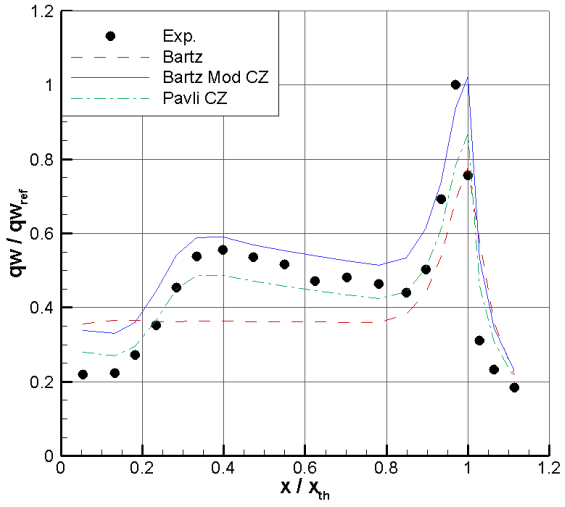

(a) Heat fluxes at $MR = 6$, $p_c = 60$ bar

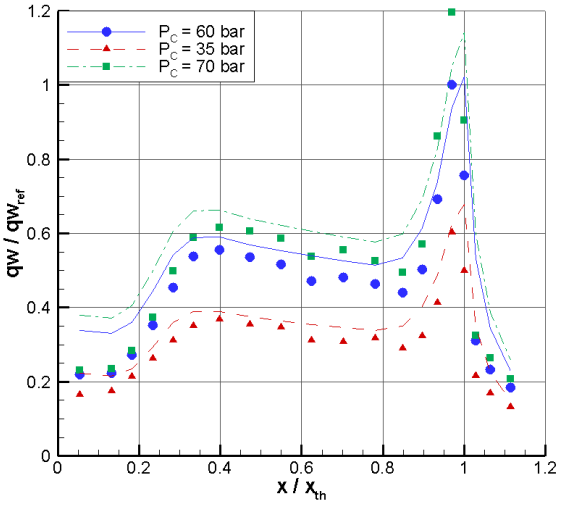

(b) Heat fluxes at $MR = 6$, $p_c = 35, 60, 70$ bar

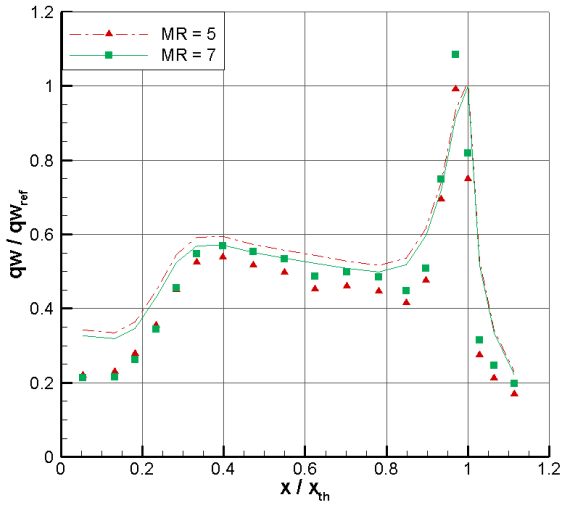

(c) Heat fluxes at $MR = 5, 7$, $p_c = 60$ bar

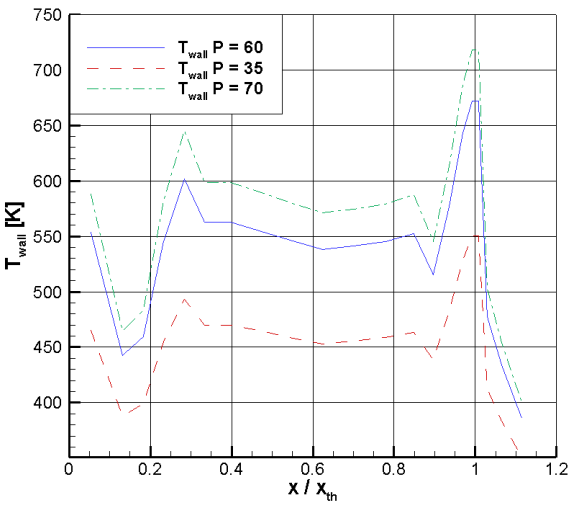

(d) Wall temperatures at $MR = 6pc = 35, 60, 70$ bar

Figure 4: Heat fluxes and wall temperatures results

require experimental data with different calorimetric chambers and different injector configurations. This is out of the scope of a 0-D/1-D engineering tool like EcosimPro.

The heat fluxes in the divergent part are always overpredicted. This is a characteristic of the Bartz model and needs to be kept in mind when interpreting the results. However, introducing the "flow acceleration" correction factor is possible to achieve a better agreement with the experimental results.

Moreover, unlike the combustion zone correction factor, its behaviour is not peculiar of the experiment considered so it can be used for different chamber configurations and performance conditions. No tuning has been performed on the Bartz and Pavli parameters, the constants have been taken as $C = 0.026$, and $C = 0.023$ respectively as recommended by Bartz and Pavli.

For each correlation, some remarks follow:

- **Simple Bartz correlation**. Here, the heat fluxes are underpredicted (around 30% in the cylindrical part) and the decreasing heat flux in the cylindrical part is not shown, but the shape of the curve in the convergent divergent nozzle region is similar to the experimental one.

- **Modified Bartz correlation**. Here, the heat fluxes are slightly overpredicted, but using the temperature and the streamwise correction it has the advantage of following very accurately the experimental data in the cylindrical part. Therefore, the model without a "combustion zone" correction factor can be applied only to part of the combustion chamber, after the mixing has taken place.

- **Pavli correlation**. This correlation is able to follow the experimental trend but in a different way of the Modified Bartz correlation. In fact, the Pavli correlation underestimates the heat fluxes while the Bartz correlation overestimates them.

- **Pressure dependency**. Using the modified Bartz correlation, test cases at different pressures have been modelled in EcosimPro. The results shown in Figure 4(b) indicate a very good agreement with experimental heat flux values. Therefore, this correlation can be considered reliable for LOX/H_2 combustion at $MR = 6$.

- **Mixture ratio dependency**. The same approach has been taken for the mixture ratio dependency. Test cases at MR varying from 5 to 7 have been modelled in EcosimPro. As can be seen in Figure 4(c), the results present a diverging behaviour. In particular, an increase in MR yields a general increase in experimental heat fluxes, while the modified Bartz correlation shows the opposite trend. It is difficult to indicate a clear explanation for these results. The main drivers for the convective heat fluxes are the mixture heat capacity at the reference temperature $c_{p,ref}$ and the temperature gradient $(T_{aw} - T_w)$. When MR increases, the heat capacity decreases (because of less hydrogen in the mixture), whereas the temperature gradient increases. In the modified Bartz model, it seems that of these two counteracting properties, the variation in $c_{p,ref}$ is predominant. In the experiment, local MR variations at the wall might be responsible for the opposed trend.

3.3 Q-2D model for cooling channels

The Q-2D model for cooling channels has been validated by comparison with a numerical test case performed by DMA [6], [7] of a turbulent flow of methane in a straight channel with asymmetric heating. These calculations have been compared with ESPSS 1D calculations and with the new Q-2D model object of this validation. The channel is smaller than the ones used in actual rocket channels. Indeed, the geometric and the boundary conditions have been chosen by DMA to obtain small values of the Reynolds number, because the computational grid size of the 3D CFD code is function of this parameter [8].

In order to validate the correct behaviour of the new transient model, two different aspect ratios of the channel have been investigated, a first channel with aspect ratio 1 and a second one with aspect ratio 8. The length and the cross section area of the channel have been kept the same among the two different channels. Both channels are 27 mm long and have a cross section of 0.08 mm^2. The boundary conditions are the same for both channels and for all models: a stagnation inlet temperature of 220 K, a stagnation inlet pressure of 90 bar, a constant temperature of 600 and 220 K at the bottom and at the top of the walls, respectively. Along the lateral side of the channel a linear temperature distribution is applied from 600 to 220 K. Figures 5(a,b) show the bulk evolution of the pressure and temperature along the channel for the aspect ratio 1 case, while Figures 5(c,d) show the pressure and temperature evolution for the aspect ratio 8 channel.

When the stratification effect is no so evident, as in the aspect ratio 1 case, the 1D model and Q-2D model have a similar trend; but when stratification occurs, as in the aspect ratio 8 channel, the differences among 1D and Q-2D model are evident, and the Q-2D results are closer to the 3D-CFD ones.

Figure 6 compares the cross-section temperature contours at the channel outlet, for each studied model and for both aspect ratios discussed here. The $AR = 1$ case features some temperature stratification in the 3D simulation. This has not been observed with the Q-2D model described in Section 2.3, which shows virtually no stratification. On the other hand, for $AR = 8$, where a consistent stratification is expected, a very good agreement can be observed between the 3D simulations and the new Q-2D model.

4 Conclusion

Three different semi-empirical models have been presented in this paper with the aim of improve the ESPSS library in the system modelling tool for transient analysis, EcosimPro.

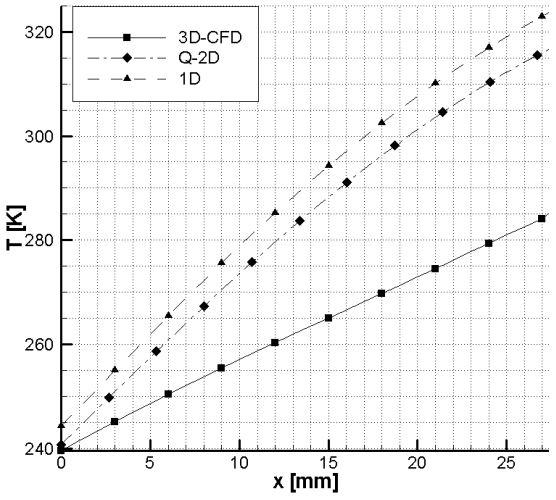

(a) Bulk temperature, $AR = 1$

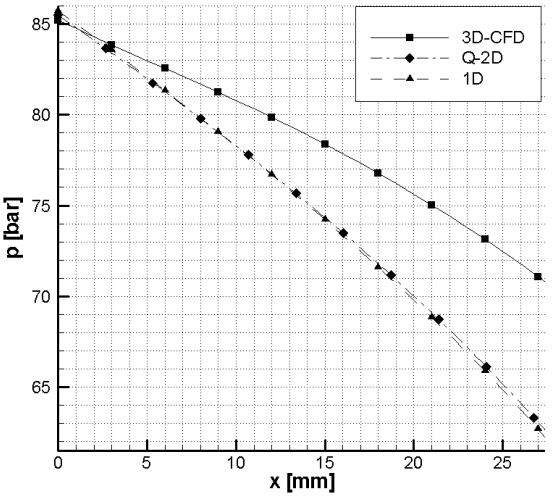

(b) Bulk pressure, $AR = 1$

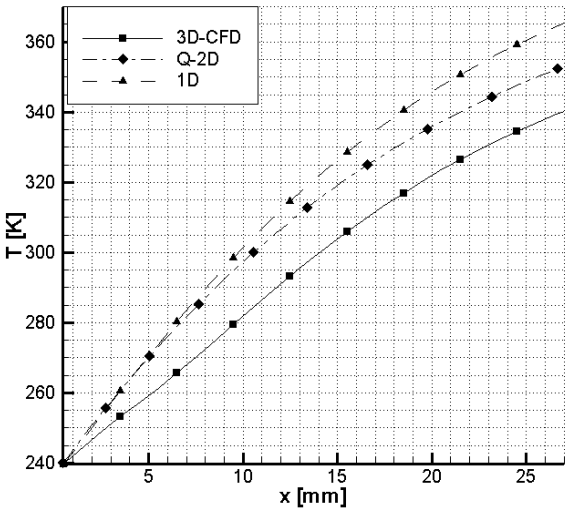

(c) Bulk temperature, $AR = 8$

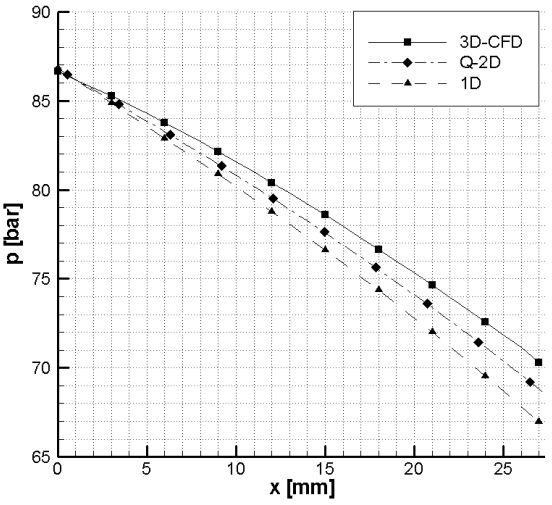

(d) Bulk pressure, $AR = 8$

Figure 5: Methane bulk variables evolution along channel axis

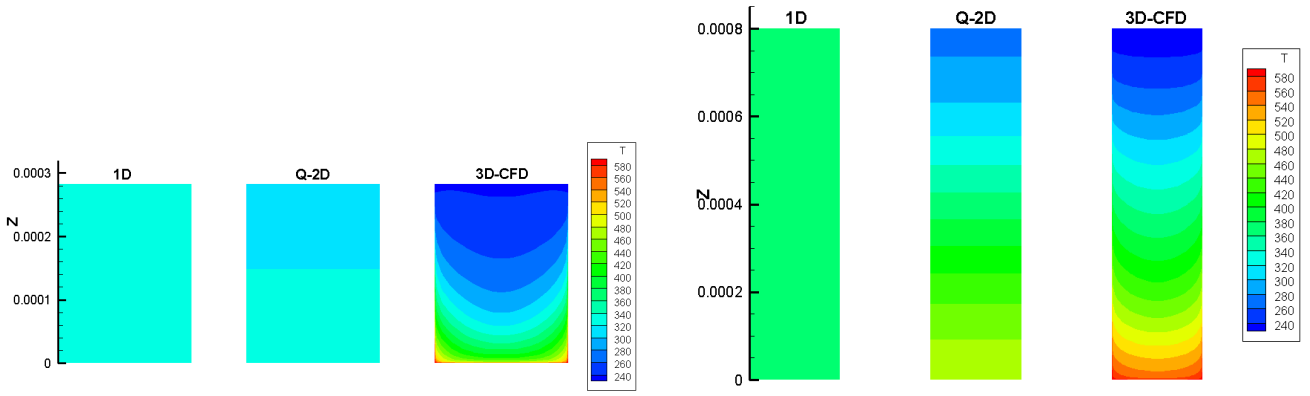

(a) Temperature stratification, $AR = 1$

(b) Temperature stratification, $AR = 8$

Figure 6: Methane temperature stratification contour plots

Each model has been developed to improve the analysis capabilities of heat transfer phenomena in the thrust chamber component. The injector head model has been tested with a realistic test case. The heat transfer correlation model has been validated with experimental data from Astrium. Finally, the quasi-2D cooling channel model has been validated by comparison with a 3D CFD study from DMA.

Future steps involve refinement and experimental validation of the injector head and quasi-2D cooling channel models.

Acknowledgements

The experimental validation data of the calorimetric combustion chamber has been kindly provided by EADS Astrium Space Transportation (Ottobrunn). The authors would like therefore to acknowledge the work of Astrium during the GSTP-2 programme with ESA, without which the implementation of the hot gas side heat transfer correlations and the comparison with experimental results would not have been possible.

Furthermore, the cooperation with M. Pizzarelli from the Department of Mechanics and Aeronautics of "Sapienza" University of Rome is acknowledged here, for the 3D CFD test cases made available for validation purposes of the quasi-2D model.

References

[1] Astrium and TU Dresden. Final report on data correlation and evaluation of test results phase 1 part 1. Internal ESA contractor report GSTP-2-TN-06-Astrium, Astrium, 2001.

[2] D. R. Bartz. Turbulent boundary-layer heat transfer from rapidly accelerating flow of rocket combustion gases and of heated air. Technical Report NASA-CR-62615, Jet Propulsion Laboratory, 1963.

[3] K. J. Kacynski. Thermal stratification potential in rocket engine coolant channels. Technical Report TM-4378, NASA, 1992.

[4] A. J. Pavli, J. K. Curley, P. A. Masters, and R. M. Schwartz. Design and cooling performance of a dump cooled rocket engine. Technical Note TN D-3532, NASA, August 1966.

[5] M. Pizzarelli, F. Nasuti, and M. Onofri. A simplified model for the analysis of thermal stratification in cooling channels. In *EUCASS, 2nd European Conference for Aerospace Sciences*, July 2007.

[6] M. Pizzarelli, F. Nasuti, and M. Onofri. Flow analysis of transcritical methane in rectangular cooling channels. In *44th AIAA/ASME/SAE/ASEE Joint Propulsion Conference and Exhibit*, number 2008-4556, July 2008.

[7] M. Pizzarelli, F. Nasuti, and M. Onofri. Investigation of transcritical methane flow and heat transfer in curved cooling channels. In *45th AIAA/ASME/SAE/ASEE Joint Propulsion Conference*, number 2009-5304, August 2009.

[8] M. Pizzarelli, F. Nasuti, R. Paciorri, and M. Onofri. Numerical analysis of three-dimensional flow of supercritical fluid in asymmetrically heated channels. *AIAA Journal*, 47(11), November 2009.

[9] D. Preclik, D. Wiedmann, W. Oechslein, and J. Kretschmer. Cryogenic calorimeter chamber experiments and heat transfer simulations. In *AIAA/ASME/SAE/ASEE 34th Joint Propulsion Conference and Exhibit*, number 98-3440, July 1998.

[10] A. Woschnak and M. Oschwald. Thermo- and fluidmechanical analysis of high aspect ratio cooling channels. In *AIAA/ASME/SAE/ASEE 37th Joint Propulsion Conference and Exhibit*, number 2001-3404, July 2001.